Nutrient-dependent trade-offs between ribosomes and division protein synthesis control bacterial growth and cell shape

Diana Serbanescu,[1] Nikola Ojkic,[1] and Shiladitya Banerjee[1,2,†]

[1] *Department of Physics and Astronomy, University College London, London WC1E 6BT, UK*

[2] *Department of Physics, Carnegie Mellon University, Pittsburgh, PA 15213, USA*

SUMMARY

Cell size control emerges from a regulated balance between the rates of cell growth and division. In bacteria, simple quantitative laws connect cellular growth rate to ribosome abundance. However, it remains poorly understood how translation regulates bacterial cell size and shapes under growth perturbations. Here we develop a whole-cell model for growth dynamics in rod-shaped bacteria that links ribosomal abundance with cell geometry, division control, and the extracellular environment. Our study reveals that cell shape maintenance under nutrient perturbations requires a balanced trade-off between ribosomes and division protein synthesis. Deviations from this trade-off relationship is predicted under translational perturbations, leading to distinct modes of cell morphological changes, in agreement with single-cell experimental data on *Escherichia coli*. Furthermore, by calibrating our model with experimental data, we predict how combinations of nutrient-, translational- and shape perturbations can be chosen to optimize bacterial growth fitness and drug resistance.

KEYWORDS

whole-cell model, bacterial growth, cell shape control, translation, antibiotics

INTRODUCTION

Cell size maintenance is essential for regulating cell physiology, function and fitness [1]. Maintaining a characteristic cell size necessitates an intricate balance between cell growth and division rates. How this balance is achieved in different growth conditions remains an outstanding question. It has been known for over six decades that bacteria modulate their size in response to changes in nutrient conditions. Quantifying the cell size and growth rates of *Salmonella enterica* grown in different nutrient media, Schaechter and colleagues discovered the *nutrient growth law* – bacterial cell size

† Correspondence: shiladtb@andrew.cmu.edu

increases exponentially with the population growth rate [2]. High-throughput single-cell studies in recent years have confirmed this result for evolutionary divergent *Escherichia coli* and *Bacillus subtilis* [3–6], suggesting common strategies for bacterial cell size control. However, single-cell data show deviations from the nutrient growth law in experiments altering cellular proteomics [4, 7], leaving open the connection between cell size, growth rate and protein synthesis.

At the single-cell level, cell size homeostasis is achieved via the *adder* mechanism, whereby cells add a constant volume between consecutive division events, irrespective of the cell size at birth [8–11]. As a result of this strategy, cells deviating from the average homeostatic size quickly converge to the average size within a few generations [5, 12–15]. This strategy for cell size homeostasis is followed by a wide range of bacterial species including *E. coli*, *B. subtilis*, *C. crescentus* and *P. aeruginosa* [11, 12, 14–16], but does not provide a molecular-level understanding of the mechanism for size control [17]. Recent studies [14, 18–20] have linked the adder model of cell size homeostasis to the accumulation of a threshold amount of division proteins (FtsZ) to trigger cell division. However, it remains unknown how the synthesis of division proteins is altered by nutrients or translational perturbations in order to regulate cell size.

A key component in understanding cell size regulation is the interdependence between growth rate and the macromolecular composition of the cell. The nutritional content of the growth medium sets the specific growth rate [2, 21], which in turn regulates the macromolecular composition of cells [22, 23]. For exponentially growing *E.coli* cells, RNA and ribosome abundance increases linearly with increasing the specific growth rate [7, 24–28]. This implies an upregulation in translation leading to increased protein production for growth [7, 29, 30] and cell size inflation. While this model is in agreement with experimental observations for cell size increase with increasing nutrient concentrations, it fails to explain cell size changes under translation inhibition [4, 7]. In particular, it remains unclear whether translation inhibition would lead to an increase in cell size such that there is a positive correlation between cell size and ribosome abundance, or a decrease in cell size with growth rate reduction. Both these behaviors are observed in experiments [4]. To explain how translation and nutrient quality regulates cell morphologies, we develop a whole-cell coarse-grained theory that links ribosomes with cell geometry, division control and the extracellular environment.

Our theoretical framework combines a mechanistic model of cell shape and division with an extended ribosomal resource allocation model, allowing us to quantitatively predict cell size changes under nutrient shifts and translational perturbations. We use ribosome abundance as the one of the key regulatory variable as approximately 85% of cellular RNA encodes for rRNA that is folded in ribosomes [31, 32]. We also assume that all the nutrients transported from the extracellular

medium into the cell are used in the production of ribosomes and other proteins. This is because over 80% of cell's energy requirements for biomass is spent on proteins and rRNA synthesis [33]. Using this framework, we uncover a model for balanced allocation of ribosomal resources towards cell growth and division. We find that a balanced trade-off between the rates of cell growth and division proteins synthesis sets bacterial size under nutrient shifts. As a result, in rich media, cells produce division proteins slower than the rate of cell elongation leading to larger cell sizes.

We then extend our framework to predict cell morphologies under translation inhibition across different nutrient media. Our model predicts three different types of cell morphological response unifying past experimental observations [4, 7, 31]. First, cells deprived of nutrients allocate more ribosomes towards growth which results in an increase in volume. Second, cells grown in rich nutrient media favor resource allocation towards division and thus a decrease in volume is observed under translation inhibition. Under optimal growth conditions cells preserve the balance between growth and division protein synthesis, such that cell size is invariant under translational perturbations. We show that cell size changes are intimately coupled to the regulation of cell surface-to-volume ratio – a fitness metric that controls nutrient and antibiotic influx rates. We therefore investigate the relationship between cell shape, nutrient quality and bacterial growth rate under translational perturbations. We predict that round cells are most resistant to translation-inhibitory antibiotics, and that drug resistance increases with increasing nutrient quality. Thus, induced filamentation could have a negative impact on bacterial growth fitness [34], whereas cell rounding could promote bacterial resistance to ribosome-targeting antibiotics.

RESULTS

Cell size control emerges from nutrient-dependent trade-off between rates of cellular growth and division protein synthesis.

To understand how bacterial cell size changes with the nutrient specific growth rate, we develop a model for the allocation of ribosomal resources towards cell growth and division protein synthesis. During each cell cycle, cells elongate exponentially in volume (V) at a rate κ. At steady-state, κ depends linearly on the ribosomal mass fraction r ($\approx$ RNA/protein ratio), such that

$$\frac{\mathrm{d}V}{\mathrm{d}t} = \kappa(r)V(t) \ , \tag{1}$$

where $\kappa(r) = \kappa_t(r - r_{\mathrm{min}})$ [31]. Here, κ_t can be interpreted as the translational capacity of the cell, which correlates with the speed of translational elongation [35], and r_{min} is the minimum mass fraction of ribosomes needed for growth (Fig. 1C inset). The value for r_{min} is obtained from the

intercept of κ as a function of r from experimental data [4, 31].

We combine this model for growth with a model for the control of cell division (Fig. 1A). The division proteins, X, are synthesised at a rate proportional to the cell volume:

$$\frac{\mathrm{d}X}{\mathrm{d}t} = k_p(r)V(t) \ , \tag{2}$$

where $k_p(r)$ is the rate of synthesis of division proteins that is assumed to be a function of the ribosome mass fraction. Cell division is triggered when a threshold copy number of division proteins, X_0, is accumulated at the mid-plane of the cell (Fig. 1B). While various proteins could be potential candidates for division initiation [36–39], a recent study identifies FtsZ as the key initiator protein that assembles a ring-like structure in the mid-cell region to trigger septation [19]. We therefore suggest that X represents FtsZ copy number, and assume that its turnover rate in the ring-bound state is much faster than its rate of synthesis [40]. As a result, all the newly synthesised FtsZ in the cytoplasm are assumed to be recruited in the ring.

Solving Eq. (1) and Eq. (2), we obtain: $X_0 = \Delta V k_p/\kappa$, where ΔV is the added volume per generation. As X_0, k_p and κ are constant for a given growth medium, cells add a constant volume ΔV in each growth generation, consistent with the phenomenological adder model. Furthermore, for symmetrically dividing bacterium, the average newborn cell volume, $\langle V \rangle$, asymptotes to ΔV [12]. Therefore, average cell volume in a given growth medium is given by the ratio of growth rate to the rate of division protein synthesis:

$$\langle V \rangle = \frac{\kappa}{\kappa_p} \ , \tag{3}$$

where $\kappa_p = k_p/X_0$, is the normalized rate of division protein synthesis. Thus, cell volume can be modulated by perturbations in translation, as both κ and κ_p are functions of the ribosomal mass fraction. A key proposition of our model is that there is a tradeoff between ribosomes allocated for synthesizing growth and division proteins such that:

$$\kappa_p = \kappa_p^0(r^*_{\mathrm{max}} - r) \ , \tag{4}$$

where κ_p^0 can be interpreted as the rate of production of FtsZ per ribosomes, and r^*_{max} is the ribosome mass fraction when growth rate is maximum. By combining the expressions for growth rate and division proteins synthesis rate, we find:

$$\langle V \rangle = \frac{\kappa_t(r - r_{\mathrm{min}})}{\kappa_p^0(r^*_{\mathrm{max}} - r)} \ , \tag{5}$$

such that average cell size increases with increasing ribosome abundance. We fit the expression in Eq. (5) to experimental data [4] in order to determine the parameters κ_p^0 and r^*_{max} (Fig. 1C). We

can then express the average volume as a function of nutrient specific growth rate, recapitulating Schaecter et al.'s *nutrient growth law* [2] that cell size increases monotonically with increasing growth rate (Fig. 1D):

$$\langle V \rangle = \frac{\kappa}{\kappa_p^0 (r^*_{\max} - r_{\min}) - \frac{\kappa_p^0}{\kappa_t}\kappa} \ . \tag{6}$$

Notably, our result deviates from the phenomenological model of exponential dependence between cell size and growth rate, and predicts a maximum growth rate, $\kappa_{\max} = \kappa_t(r^*_{\max} - r_{\min}) \approx 3.1\text{h}^{-1}$, when all ribosomal resources are allocated towards growth.

To understand the mechanistic origin of the ribosomal tradeoff between growth and division protein synthesis (Eq. 4), we consider a model for allocation of ribosomal resources, extending the framework of Scott et al [31]. The total protein content of the cell can be decomposed into four classes (Fig. 1E): ribosome-affiliated proteins (R, mass fraction ϕ_R), house-keeping proteins not affected by translation (Q, mass fraction ϕ_Q), division proteins (X, mass fraction ϕ_X), and the rest non-ribosomal proteins (P, mass fraction ϕ_P). The mass fractions are constrained by the equation: $\phi_R + \phi_X + \phi_P = 1 - \phi_Q = \phi_R^{\max} =$ constant. For different combinations of the nutritional and translation capacities of the cell, efficient resource allocation requires that the abundance of P- and R-class proteins be adjusted so that the rate of nutrient influx by P matches the rate of protein synthesis achievable by R: $\kappa_n \phi_P = \kappa_t(\phi_R - \phi_R^{\min})$, where κ_n is the nutritional capacity of the cell. This results in the following relation between the mass fractions of ribosomes and division proteins:

$$\frac{\phi_R - \phi_R^{\min}}{\phi_R^{\max} - \phi_R - \phi_X} = \frac{\kappa_n}{\kappa_t} \ . \tag{7}$$

We assume that the rate of production of division proteins, κ_p, is proportional to ϕ_X: $\kappa_p = \lambda \phi_X$, and $r = \phi_R/\rho$, where ρ and λ are constant conversion factors. This results in Eq. (4),

$$\kappa_p = \frac{\lambda\rho(\kappa_n + \kappa_t)}{\kappa_n} \left(\frac{\kappa_n \phi_R^{\max} + \kappa_t \phi_R^{\min}}{\rho(\kappa_n + \kappa_t)} - r \right) \ , \tag{8}$$

where we identify $\kappa_p^0 = \lambda\rho(\kappa_n + \kappa_t)/\kappa_n$, and $r^*_{\max} = (\kappa_n \phi_R^{\max} + \kappa_t \phi_R^{\min})/\rho(\kappa_n + \kappa_t)$. Growth rate κ decreases with increased allocation of resources towards division proteins ϕ_X (Fig. 1E-F):

$$\kappa = \frac{\kappa_n \kappa_t}{\kappa_n + \kappa_t} (\phi_R^{\max} - \phi_R^{\min} - \phi_X)/\rho \ . \tag{9}$$

With all the model parameters inferred from experimental data (Methods, Table 1), we can plot the dependency of κ_p on κ (Fig. 1F), showing the negative correlation between the division protein synthesis rate and the volumetric growth rate. Cells growing in poor nutrient medium allocate a smaller fraction of ribosomes towards growth, resulting in smaller size on average. However,

cells growing in rich nutrients inflate their size by allocating a larger fraction of ribosomes towards growth (Fig. 1E).

Translation inhibition breaks balanced allocation of ribosomal resources.
In a given nutrient medium, κ/κ_p is maintained at a constant value, indicating a balance between growth and division protein synthesis. If κ/κ_p remains invariant under translation inhibition, we expect cell size to remain unchanged, as previously suggested by Basan *et al.* [7]. However, experimental data [4] show that cell size could either increase, decrease or remain unchanged when *E. coli* cells are subjected to varying concentrations of Chloramphenicol – a ribosome-targeting antibiotic. We therefore hypothesize that translation inhibition breaks balanced allocation of ribosomal resources towards growth and division proteins, by differentially reducing the rates κ and κ_p.

Under translation inhibition, bacteria produce more ribosomes to compensate for the inactive ribosomes that are bound by antibiotics [31]. By measuring bacterial growth rates and ribosome mass fractions for increasing concentrations of Chloramphenicol, Scott *et al.* [31] obtained:

$$\kappa = \kappa_n(r_{\max} - r) \ , \tag{10}$$

where κ_n is the nutritional capacity that depends on nutrient quality, and $r_{\max}$ is the maximum ribosome fraction that cells can produce under translation inhibition, weakly correlating with the nutrient specific growth rate [31]. By combining Eq. (10) with Eq. (4), we find:

$$\kappa_p = \kappa_p^0(\kappa/\kappa_n + \delta r) \tag{11}$$

where $\delta r = r^*_{\max} - r_{\max}$ can be interpreted as the excess ribosomal mass fraction allocated to division protein synthesis under translation inhibition. Unlike nutrient perturbations, we find that κ_p and κ are positively correlated under translation inhibition (Fig. 2A), such that they both decrease with increasing antibiotic concentration. Eq. (11) can be combined with Eq. (3) to determine how cell volume changes as a function of growth rate under translation inhibition:

$$\langle V \rangle = \frac{\kappa/\kappa_p^0}{\kappa/\kappa_n + \delta r} \ . \tag{12}$$

Interestingly, the above expression predicts three distinct behaviors (Fig. 2B):

$$\begin{cases} \delta r > 0 \rightarrow r^*_{\max} > r_{\max} : \text{more ribosomes allocated to division, cell volume decreases} \\ \delta r = 0 \rightarrow r^*_{\max} = r_{\max} : \text{ribosomes equally shared between growth and division, volume unchanged} \\ \delta r < 0 \rightarrow r^*_{\max} < r_{\max} : \text{excess ribosomes allocated to growth, volume increases.} \end{cases}$$

We determine the parameters δr and κ_n for each growth medium, by fitting Eq. (11) to the experimental data for cell growth rate and volume under Chloramphenicol perturbations [4] (Fig. 2C). We find that $\delta r < 0$ in poor media, $\delta r > 0$ in rich growth media, whereas $\delta r \approx 0$ for cells growing with medium growth rates (Fig. 2D). We interpret the above result as cells allocating excess ribosomes for growth in poor media, whereas in rich media cells tend to allocate more ribosomal resources for division protein synthesis. The predicted volume curves for each growth conditions quantitatively capture the trend in the experimental data without further fitting (Fig. 2E).

Cells actively regulate shapes to adapt to translational perturbations.
Under translation inhibition, decrease in cell volume in rich media is indicative of a higher surface-to-volume ratio that may drive an increased nutrient influx. Conversely, in poor media, increase in cell volume may be indicative of a lower surface-to-volume ratio that in turn would reduce antibiotic influx (Fig. 2F). Therefore the surface-to-volume ratio of the cell may play a crucial role in controlling cellular adaptive response to perturbations in the growth medium. To test this hypothesis, we construct a model coupling cell growth and geometry to nutrient and antibiotic transport.

Nutrient dynamics. The dynamics of nutrient concentration inside the cell, $[n]$, is given by:

$$\frac{d[n]}{dt} = J_n - \kappa[n] - \kappa_r r_a \tag{13}$$

where $J_n = [n_{\text{ext}}]P_{\text{in}}A/V$ is the nutrient influx, $[n_{\text{ext}}]$ is the nutrient concentration in the extracellular medium, P_{in} is the cell envelope permeability and κ_r is the rate at which ribosomes are produced from the nutrients. The model for nutrient transport across the cell membrane is consistent with the one proposed in [41] if we assume that the number of metabolic proteins (transporters) scales with the surface area of the cell. The interplay between nutrients and ribosome synthesis is schematically represented in Fig. 3A. The intracellular concentration of nutrients determines the specific growth rate as: $\kappa_{\text{specific}} = \kappa_0[n]/([n] + n^*)$ [42], where κ_0 is the maximum growth rate characteristic of the medium, and n^* is the value of $[n]$ when $\kappa_{\text{specific}}/\kappa_0 = 0.5$. When the nutrients inside the cell reach saturation, i.e. $\mathrm{d}[n]/\mathrm{d}t = 0$, $\kappa = \kappa_{\text{specific}}$.

Antibiotic dynamics. The action of ribosome-targeting antibiotics is illustrated using the diagram in Fig. 3A, which consists of two key components: the flux of antibiotics J_a entering the cell, and the binding of antibiotics to the active pool of ribosomes, r_a. The dynamics are described by the

following set of equations, extending the model of Elf *et al.* [43] and Greulich *et al.* [44],

$$\begin{cases} da_{\text{in}}/dt &= -\kappa a_{\text{in}} + f(r_a, r_b, a_{\text{in}}) + J_a(a_{\text{ex}}, a_{\text{in}}, A, V), \\ dr_a/dt &= -\kappa r_a + f(r_a, r_b, a_{\text{in}}) + s, \\ dr_b/dt &= -\kappa r_b - f(r_a, r_b, a_{\text{in}}), \end{cases} \tag{14}$$

where a_{ex} is the extracellular antibiotic concentration, a_{in} is the intracellular concentration of the antibiotic, r_a is the concentration of the active pool of ribosomes in the cell, r_b is concentration of the pool of ribosomes bound by the antibiotics, and s is the rate of synthesis of ribosomes. Unlike previous models [43, 44], here we account for the dependence of J_a on cell shape as:

$$J_a(a_{\text{ex}}, a_{\text{in}}, A, V) = (P_{\text{in}} a_{\text{ex}} - P_{\text{out}} a_{\text{in}}) \frac{A}{V}, \tag{15}$$

where P_{in} and P_{out} are the cell envelope permeabilities in the inward and outward directions, respectively. The ribosome-antibiotic interactions are defined by: $f(r_a, r_b, a_{\text{in}}) = -k_{\text{on}} a_{\text{in}}(r_a - r_{\text{min}}) + k_{\text{off}} r_b$, where k_{on} is the rate of binding of antibiotics to ribosomes, and k_{off} is the rate of unbinding. These rate constants for Chloramphenicol are known from literature [43, 44]. Furthermore, cells produce more ribosomes to compensate for the inactive ribosomes bound by antibiotics [31]. This is captured by the source term: $s = \kappa(r_{\text{max}} - \kappa \Delta r(1/\kappa_{\text{specific}} - \kappa_t/\Delta r))$, where $\Delta r = r_{\text{max}} - r_{\text{min}}$.

Cell shape dynamics. Having described the dynamics of cell volume (Eq. 1), division control (Eq. 2), nutrient and antibiotic transport (Eq. 13-14), we need to additionally account for cell surface area synthesis to predict cell shape changes. We assume that rate of synthesis cell surface area is proportional to cell volume [45]:

$$\frac{\text{dA}}{\text{d}t} = \beta V(t) \ , \tag{16}$$

where β is the rate of surface area production, which depends on cell shape, growth rate and division protein synthesis rate. Solving Eq. (1) and Eq. (16), one obtains $A/V = \beta/\kappa$, at steady-state [45]. In recent work [20] we found that *E. coli* cells obey the relation: $A = \nu V^{2/3}$, under nutrient and translational perturbations, where ν is a geometric factor related to the cell aspect ratio η as: $\nu = \eta\pi(\frac{\eta\pi}{4} - \frac{\pi}{12})^{-2/3}$. Therefore, surface area production rate varies non-monotonically with growth rate as: $\beta = \nu\kappa(\kappa/\kappa_p)^{-1/3}$ (Fig. 3B).

Taken together, our model accounts for the key functions of ribosomes in controlling cell growth rate (κ), rate of production of division proteins (κ_p), and the rate of surface area synthesis (β). Under translation inhibition, both κ and κ_p decreases as shown in Fig. 2A and C. Surface area production rate is also impacted by translation inhibition, as shown in Fig. 3B, albeit in a different

manner from the growth rate. Differential reduction of κ and β under translation inhibition is indicative of changes in steady-state cell surface-to-volume ratio ($\propto \beta/\kappa$). To test this quantitatively, we simulated the coupled equations (Methods) for single-cell growth (Eq. 1, 2 and 16), nutrient (Eq. 13) and ribosome-antibiotic dynamics (Eq. 14) under stresses induced by ribosome-targeting antibiotics (Fig. 3C). In response to a step pulse of antibiotic in a rich nutrient medium at $t = 0$ h, the concentration of antibiotic inside the cell and the influx increase rapidly. This in turn reduce cell elongation rate as a result of antibiotic binding to ribosomes, and leads to longer interdivision times, a decreased (increased) average birth volume and a concomitant increase (decrease) in surface-to-volume ratio for cells growing in rich (poor) nutrients. These results confirm our hypotheses that in poor media, cells reduce their surface-to-volume ratio to inhibit antibiotic influx, while in rich media cells increase their surface-to-volume ratio to import more nutrients.

While all the model parameters can be calibrated from available experimental data (Table 1), the relative magnitude of the permeabilities, $P_{\text{in}}/P_{\text{out}}$ remains undetermined. To this end, we fit our model to the experimental growth-inhibition curves [4] in differents nutrient conditions (Fig. 3D), treating $P_{\text{in}}/P_{\text{out}}$ as a fitting parameter. Interestingly, we find that $P_{\text{in}}/P_{\text{out}}$ is nutrient-dependent and decreases with increasing specific growth rate (Fig. 3E). Including nutrient-dependent regulation of membrane permeability, our model predictions capture the experimental data for the decrease in division protein synthesis rate under Chloramphenicol inhibition (Fig. 3F) and the changes in cell volume (Fig. 3G). Consistent with our hypothesis and experimental data, we find that cell surface-to-volume increases in rich nutrient media (synthetic rich in experiments), suggestive of increased nutrient influx (Fig. 3H). Conversely, in poor nutrient medium (glycerol in experiments), cell surface-to-volume reduces with increasing drug dosage, suggesting that cells are countering the influx of antibiotics if sufficient nutrients are not available.

Nutrient-dependent regulation membrane permeability to antibiotics (Fig. 3E) can be a result of different metabolic pathways. It has been observed that *E.coli* cells have different metabolic pathways for nutrients depending on the growth conditions [46]. Furthermore, if the cells are subjected to a nutrient downshift, the proteome reallocates such that a larger fraction of proteins is allocated to the sector responsible for carbon catabolism which in turn reduces the available proteome fraction for other sectors [47, 48]. The transition from one metabolic mechanism to another can be justified using a proteome allocation model as suggested by Basan *et al.* [48] and Mori *et al.* [47], or by increasing the glucose uptake rates. The drop in cell envelope permeability that we observe around $\kappa = 0.6$ h^{-1} (Fig. 3E) matches the maximum growth rate that *E.coli* cells can achieve while staying below the critical limit on energy dissipation [49].

Cell surface area production promotes bacterial growth inhibition by ribosome-targeting antibitiocs.

Our theory predicts that bacterial growth response to translation-inhibitory antibiotics is governed by nutrient-dependent cell shape changes (Fig. 2-3). To systematically study how bacterial growth inhibition depends on cell shape and nutrient quality, we simultaneously perturbed cell shape and ribosomal translation in varying growth media using our computational model. These simulations can be realised experimentally by simultaneously applying two antibiotics - one that changes cell shapes (e.g. by targeting the cell wall), while the other affects the translational machinery by inhibiting ribosomal activity. The resultant effect can be suppressive, antagonistic, or synergistic depending on what the combined effect of the two drugs is with respect to the individual effect of each [50, 51].

In simulations we simultaneously applied a surface area *modifier* and chloramphenicol to a cell growing at steady-state. To achieve rounder cells, the *modifier* is a surface area synthesis inhibitor that decreases the surface production rate β, by decreasing the cell's geometric factor ν ($= A/V^{2/3}$), which in turn reduces cellular aspect ratio. By contrast, long filamentous cells are obtained when a surface area promoter is added (increasing ν), leading to higher aspect ratio cells.

We investigated the response of growth rate to increasing Chloramphenicol concentrations for cells with varying aspect ratios – ranging from $\eta = 1$ for coccoidal cells to $\eta = 10$ for filamentous cells (Fig. 4A). The response of κ to the concentration of the applied antibiotic can be characterized by a Hill function of the form [52] (Fig. 4A):

$$\kappa(a_{\text{ex}}) = \frac{\kappa_{\text{specific}}}{1 + (\frac{a_{\text{ex}}}{\text{IC}_{50}})^n} \ , \tag{17}$$

where IC_{50} is the half-inhibitory concentration of the antibiotic, and the Hill coefficient n quantifies the dose-sensitivity of the growth rate to relative changes in drug concentration. We take IC_{50} as a measure of drug *resistance* [52].

For a range of aspect ratios and nutrient conditions, we fitted the growth inhibition curves to the Hill function in Eq. (17), and obtained the values for IC_{50} (Fig. 4B) and the dose-sensitivity n (Fig. 4C). Our model predicts that IC_{50} (resistance) increases with decreasing aspect ratio in rich-nutrient medium, while being less sensitive to changes in cell aspect ratio in poor-nutrient medium (Fig. 4B). Dose-sensitivity to changes in drug concentration increases with decreasing aspect ratio and increasing nutrient quality (Fig. 4C), such that dose-sensitivity is positively correlated with drug resistance (Fig. 4D). These results indicate that cellular response to translation inhibitory

antibiotics is sensitive to both the nutrient quality as well as cell shape. We find that round coccoidal cells are most drug-resistant, while filamentous cells are least resistant (Fig. 4E). Furthermore, depending on nutrient-quality, cellular morphological response to translation inhibitory drugs is different. While cells increase their surface-to-volume ratio to import more nutrients in nutrient-poor medium, cells prefer to reduce their surface-to-volume ratio in rich-nutrient medium to inhibit antibiotic influx (Fig. 2-3). These findings predict that bacterial growth inhibition can be maximized by simultaneously inhibiting ribosomal translation and promoting surface area production in nutrient-poor media.

DISCUSSION

We develop a whole-cell coarse-grained model for bacterial growth dynamics that connects intracellular control of translation, with cell shape, division control and extracellular environment. This provides a promising theoretical framework that quantitatively captures available experimental data for bacterial cell size and shape dynamics under nutrient and translational perturbations. Out study reveals that during nutrient shifts, the ribosomal resources are optimally allocated to maintain a balanced trade-off between the rates of cell growth and division protein synthesis. In rich nutrient media, more ribosomes are used for growth than division protein synthesis, leading to cell size inflation with increasing nutrient quality. Conversely in nutrient-poor media, cells allocate more ribosomal resources for division protein synthesis than growth, leading to a reduction in average cell size. This principle underlies the molecular basis for the celebrated *nutrient growth law* [2, 4], and can be interpreted as an optimization principle for cellular economy. Based on this principle, the resources allocated to a particular proteomic sector are inversely proportional to the efficiency of that sector [41]. In nutrient-rich media, cells invest more ribosomal resources to growth in order to compensate for a lower translational capacity. The latter can arise from an increased dilution rate of ribosomes under fast growth conditions, lowering the efficiency of protein synthesis. In nutrient-poor media, cells have a lower nutritional capacity that they compensate by allocating more resources to metabolism and division protein synthesis.

Comparing our theory to experimental data, we uncover several feedback pathways between cell shape, growth rate, protein synthesis and extracellular transport that were previously unknown (Fig. 4F). In particular, we predict that under translation inhibition, cells break the balanced trade-off between ribosomes and division protein synthesis, leading to cell size inflation, reduction or size invariance, in a nutrient-dependent manner. Our model predictions are in quantitative agreement with experimental data on *E. coli* cells subjected to Chloramphenicol perturbations across various

nutrient conditions [4]. If cells are grown in nutrient-rich media, the excess ribosomes produced under translation inhibition are allocated towards division, leading to smaller cell sizes and higher surface-to-volume ratios. This is in agreement with Chloramphenicol treated *E.coli* cells grown in synthetic rich medium. Conversely, in nutrient-poor media cells allocate excess ribosomes towards growth, leading to cell size inflation and lower surface-to-volume ratios, in agreement with *E.coli* cell data in glycerol medium. This suggests that cells shape changes in response to translation-inhibitory antibiotics may confer certain fitness advantages under stress. In nutrient-rich media it is more favorable for cells to reduce their surface-to-volume in order to minimize antibiotic influx. Whereas in nutrient-poor media, cells adapt to import more nutrients by increasing their surface-to-volume ratios.

To quantitatively test the role of cell shape and nutrient quality on bacterial growth inhibition under antibiotic stress, we simulated bacterial growth under simultaneous perturbation of surface area production and translation inhibition in varying nutrient media. From growth-inhibition curves we measured bacterial response to antibiotics by quantifying resistance (half-inhibitory concentration of the drug) and dose-sensitivity to increasing concentration of the drug. Our study reveals that that round-shaped cells are fitter and more drug-resistant than higher aspect ratio filamentous cells, and that dose-sensitivity increases with increasing nutrient quality. These results can be tested experimentally by measuring bacterial growth rates in response to simultaneous application of cell-wall targeting and ribosome-targeting antibiotics, in different nutrient concentrations. Interestingly, we predict that bacterial growth-inhibition can be maximized by simultaneously inhibiting ribosomal translation and promoting surface area production in nutrient-poor media.

ACKNOWLEDGMENTS

We thank Suckjoon Jun lab (UCSD) for providing single cell shape data for *E. coli*, and Guillaume Charras for many useful discussions. SB acknowledges funding from EPSRC grant EP/R029822/1, Royal Society grants URF/R1/180187 and RGF/EA/181044.

AUTHOR CONTRIBUTIONS

SB and DS designed research. DS, NO and SB developed theory. DS performed simulations and analysed data. DS and SB wrote the paper.

DECLARATION OF INTERESTS

The authors declare no competing interests.

Table 1. **List of parameters used in the model and simulations.**

Parameter	Value	Growth medium	Expression/method	Figure number
$r_{\min}$	0.1	all	$\kappa = \kappa_t(r - r_{\min})$	1, 2, 3, 4
$\kappa_t(\mathrm{h}^{-1})$	5.6	all		
$\kappa_p^0(\mathrm{h}^{-1}\mu\mathrm{m}^{-3})$	2.1	all	$V = \frac{\kappa_t(r-r_{\min})}{\kappa_p^0(r^*_{\max}-r)}$	1, 2, 3, 4
$r^*_{\max}$	0.7	all		
$r_{\max}$	0.7	all	$\kappa = \kappa_n(r_{\max} - r)$	2, 3, 4
$\kappa_n(\mathrm{h}^{-1})$	9.1	TSB	$\kappa_p = \frac{\kappa_p^0}{\kappa_n}\kappa + \kappa_p^0\delta r$	2,3,4
	8.9	synthetic rich		
	3.4	glucose + 12a.a.		
	3.5	casamino acid		
	3.4	glucose + 6a.a.		
	2.2	glucose		
	1.1	glycerol		
	1.6	sorbitol		
	1.4	mannose		
δr	0.37	TSB	$\kappa_p = \kappa_p^0(r_{\max} + \delta r - r)$	2,3,4
	0.13	synthetic rich		
	-0.18	glucose + 12a.a.		
	0.08	casamino acid		
	-0.04	glucose + 6a.a.		
	0.07	glucose		
	-0.1	glycerol		
	-0.4	sorbitol		
	-0.43	mannose		
$\kappa_r(\mathrm{h}^{-1})$	0.6	all	calibrated	3,4
$\kappa_0(\mathrm{h}^{-1})$	3	all	calibrated	3,4
$n^*(\mu\mathrm{M})$	200	all		3,4
$[n_{\mathrm{ext}}](\mu\mathrm{M})$	20	TSB		3,4
	8	synthetic rich		
	3	glucose + 12a.a.		
	5	casamino acid		
	1.8	glucose + 6a.a.		
	0.8	glucose		
	0.2	glycerol		

Table 2. **List of parameters used in the model and simulations.**

Parameter	Value	Growth medium	Expression/method	Figure number
$P_{\text{in}}/P_{\text{out}}$	0.45	TSB	Fitting growth inhibition curves	3,4
	0.80	synthetic rich		
	0.88	glucose + 12a.a.		
	0.80	casamino acid		
	0.85	glucose + 6a.a.		
	1.6	glucose		
	2.1	glycerol		
	10	sorbitol		
	15	mannose		
$k_{\text{on}}(\mu\text{M h}^{-1})$	10	all	from literature [44]	3,4
$k_{\text{off}}(\mu\text{M h}^{-1})$	25	all	from literature [44]	3,4

METHODS

Cell growth simulations. To investigate the dynamic response of cell shape and growth to applied antibiotic and nutrient shifts, we simulated single-cell growth over multiple generations. We first initiated cells at different stages in their cell cycle, and upon division followed the daughter cells over a number of generations until steady-state is reached. During each cell generation i, we evolved the following seven coupled differential equations for cell volume V_i, division protein abundance X_i, surface area A_i, nutrient concentration inside the cell $[n_i]$, antibiotic concentration inside the cell a^i_{in}, active ribosomes r^i_a, and inactive or antibiotic-bound ribosomes, r^i_b.

$$\frac{dV_i}{dt} = \kappa(r^i_a)V_i(t), \tag{18}$$

$$\frac{dX_i}{dt} = \kappa_p(r^i_a)V_i(t), \tag{19}$$

$$\frac{dA_i}{dt} = \beta(r^i_a)V_i(t), \tag{20}$$

$$\frac{d\left[n_i\right]}{dt} = J_n(\left[n_i\right], A_i, V_i) - \kappa(r^i_a)[n_i] - \kappa_r r^i_a, \tag{21}$$

$$\frac{da^i_{\text{in}}}{dt} = -\kappa(r^i_a)a^i_{\text{in}} + f(a^i_{\text{in}}, r^i_a, r^i_b) + J_a(a^i_{\text{in}}, \left[n_i\right], A_i, V_i), \tag{22}$$

$$\frac{dr^i_a}{dt} = -\kappa(r^i_a)r^i_a + f(a^i_{\text{in}}, r^i_a, r^i_b) + s(r^i_a, [n_i]), \tag{23}$$

$$\frac{dr_b^i}{dt} = -\kappa(r_a^i)r_b^i - f(a_{\text{in}}^i, r_a^i, r_b^i). \tag{24}$$

In the above equations, we have (dropping $'i'$ for simplicity):

$\kappa(r_a) = \kappa_t(r_a - r_{\min})$.

$\kappa_p(r_a) = \kappa_p^0(r_{\max}^* - r_a)$.

$\beta(r_a) = \nu[\kappa(r_a)]^{2/3}[\kappa_p(r_a)]^{1/3}$.

$J_n(A, V, [n]) = [n_{\text{ext}}]P_{\text{in}}([n])A/V$, where $[n_{\text{ext}}]$ is the extracellular nutrient concentration, and $P_{\text{in}}([n])$ is the nutrient-dependent inward permeability (Fig. 3E)

$f(a_{\text{in}}, r_a, r_b) = -k_{\text{on}}a_{\text{in}}(r_a - r_{\min}) + k_{\text{off}}r_b$.

$J_a(a_{\text{in}}, [n], A, V) = (P_{\text{in}}([n])a_{\text{ex}} - P_{\text{out}}a_{\text{in}})A/V$.

$s(r_a, [n])) = \kappa(r_a)(r_{\max} - \kappa(r_a)(r_{\max} - r_{\min})(\kappa_{\text{specific}}([n])^{-1} - \kappa_t/(r_{\max} - r_{\min}))$.

$\kappa_{\text{specific}}([n]) = \kappa_0[n]/([n] + n^*)$.

For each cell cycle i, Eq. (18)-(24) are evolved for $t \leq \tau_i$, where τ_i is the interdivision time for the ith generation. Division is triggered when $X_i > X_0$, with X_0 a constant. Upon division, we set: $V_{i+1}(0) = D_R V_i(\tau_i)$, $X_{i+1}(0) = 0$, $A_{i+1}(0) = D_R A_i(\tau_i)$, $[n_{i+1}](0) = [n_i](\tau_i)$, $a_{\text{in}}^{i+i}(0) = a_{\text{in}}^i(\tau_i)$, $r_a^{i+1}(0) = r_a^i(\tau_i)$, $r_b^{i+1}(0) = r_b^i(\tau_i)$, where D_R is a Gaussian random variable with mean 0.5 and standard deviation 0.05. We initialize the nutrient concentration inside the cell ($[n_i]$) close to zero, and calibrate the extracellular nutrient concentration $[n_{\text{ext}}]$ to reach the growth rate of the medium we choose to simulate. Over time $[n_i]$ reaches the steady-state value $n^*\kappa_{\text{specific}}/(\kappa_0 - \kappa_{\text{specific}})$, such that $\kappa = \kappa_{\text{specific}}$. We run simulations for additional 5h after the nutrient concentration reaches steady-state, to record the average values of cell volume, area, and ribosome concentration. Antibiotic perturbation is applied after 10h from the start of the simulations and continued for another 20h, when we compute the average values for the various cellular variables.

Model parameters. We extracted the parameters κ_t and $r_{\min}$ by fitting the equation $\kappa = \kappa_t(r - r_{\min})$ to the data for growth rate vs RNA/protein ratio [4] (Table 1). Using our theoretical model, we obtained the expression for cell volume V as a function of r (Eq. (5)), which we fitted to experimental data [4], in order to to extract the parameters κ_p^0, and $r_{\max}^*$ (Table 1). For cells under Chloramphenicol stress, the nutrient-dependent parameters κ_n and δr were obtained by fitting Eq. (10) and Eq. (11) to the experimental dataset for each nutrient condition (Table 1). From experimental data [4], we estimated the division protein production rate as $\kappa_p = \kappa/V$. To determine the permeability of the cell envelope to nutrient and antibiotic transport, we fitted the

growth inhibition curves resulting from our simulations to the growth inhibition curves from the data in [4], using a method of least-squares. We find that $P_{\text{in}}/P_{\text{out}}$ is a function of nutrient quality, and used that as an input to our model simulations. Tables 1 and 2 list a complete set of parameter values used in our model simulations.

REFERENCES

[1] Kevin D Young. The selective value of bacterial shape. *Microbiol. Mol. Biol. Rev.*, 70(3):660–703, 2006.

[2] M. Schaechter, O. MaalØe, and N. O. Kjeldgaard. Dependency on Medium and Temperature of Cell Size and Chemical Composition during Balanced Growth of Salmonella typhimurium. *Microbiology*, 19(3):592–606, 1958.

[3] Stephen Vadia and Petra Anne Levin. Growth rate and cell size: a re-examination of the growth law. *Current Opinion in Microbiology*, 24:96–103, April 2015.

[4] Fangwei Si, Dongyang Li, Sarah E. Cox, John T. Sauls, Omid Azizi, Cindy Sou, Amy B. Schwartz, Michael J. Erickstad, Yonggun Jun, Xintian Li, and Suckjoon Jun. Invariance of Initiation Mass and Predictability of Cell Size in Escherichia coli. *Current Biology*, 27(9):1278–1287, May 2017.

[5] Sattar Taheri-Araghi. Self-Consistent Examination of Donachie's Constant Initiation Size at the Single-Cell Level. *Frontiers in Microbiology*, 6, December 2015.

[6] John T Sauls, Sarah E Cox, Quynh Do, Victoria Castillo, Zulfar Ghulam-Jelani, and Suckjoon Jun. Gram-positive and Gram-negative Bacteria Share Common Principles to Coordinate Growth and the Cell Cycle at the Single-cell Level. *bioRxiv*, page 726596, 2019.

[7] Markus Basan, Manlu Zhu, Xiongfeng Dai, Mya Warren, Daniel Sévin, Yi-Ping Wang, and Terence Hwa. Inflating bacterial cells by increased protein synthesis. *Molecular Systems Biology*, 11(10), 2015.

[8] Mats Wallden, David Fange, Ebba Gregorsson Lundius, Özden Baltekin, and Johan Elf. The Synchronization of Replication and Division Cycles in Individual E. coli Cells. *Cell*, 166(3):729–739, July 2016.

[9] Ariel Amir. Cell Size Regulation in Bacteria. *Physical Review Letters*, 112(20):208102, May 2014.

[10] Shiladitya Banerjee, Klevin Lo, Matthew K. Daddysman, Alan Selewa, Thomas Kuntz, Aaron R. Dinner, and Norbert F. Scherer. Biphasic growth dynamics control cell division in Caulobacter crescentus. *Nature Microbiology*, 2(9):17116, September 2017.

[11] Sattar Taheri-Araghi, Serena Bradde, John T. Sauls, Norbert S. Hill, Petra Anne Levin, Johan Paulsson, Massimo Vergassola, and Suckjoon Jun. Cell-Size Control and Homeostasis in Bacteria. *Current Biology*, 25(3):385–391, February 2015.

[12] Suckjoon Jun and Sattar Taheri-Araghi. Cell-size maintenance: universal strategy revealed. *Trends in Microbiology*, 23(1):4–6, January 2015.

[13] John T Sauls, Dongyang Li, and Suckjoon Jun. Adder and a coarse-grained approach to cell size homeostasis in bacteria. *Current Opinion in Cell Biology*, 38:38–44, February 2016.

[14] Maxime Deforet, Dave van Ditmarsch, and João B. Xavier. Cell-Size Homeostasis and the Incremental Rule in a Bacterial Pathogen. *Biophysical Journal*, 109(3):521–528, August 2015.

[15] Manuel Campos, Ivan V. Surovtsev, Setsu Kato, Ahmad Paintdakhi, Bruno Beltran, Sarah E. Ebmeier, and Christine Jacobs-Wagner. A Constant Size Extension Drives Bacterial Cell Size Homeostasis. *Cell*, 159(6):1433–1446, December 2014.

[16] Matteo Osella, Eileen Nugent, and Marco Cosentino Lagomarsino. Concerted control of *Escherichia* coli cell division. *Proceedings of the National Academy of Sciences*, 111(9):3431–3435, March 2014.

[17] Suckjoon Jun, Fangwei Si, Rami Pugatch, and Matthew Scott. Fundamental Principles in Bacterial Physiology - History, Recent progress, and the Future with Focus on Cell Size Control: A Review. *Reports on Progress in Physics*, 81(5):056601, May 2018.

[18] Khem Raj Ghusinga, Cesar A. Vargas-Garcia, and Abhyudai Singh. A mechanistic stochastic framework for regulating bacterial cell division. *Scientific Reports*, 6(1):30229, September 2016.

[19] Fangwei Si, Guillaume Le Treut, John T. Sauls, Stephen Vadia, Petra Anne Levin, and Suckjoon Jun. Mechanistic Origin of Cell-Size Control and Homeostasis in Bacteria. *Current Biology*, 29(11):1760–1770.e7, June 2019.

[20] Nikola Ojkic, Diana Serbanescu, and Shiladitya Banerjee. Surface-to-volume scaling and aspect ratio preservation in rod-shaped bacteria. *eLife*, 8:e47033, August 2019.

[21] Matthew Scott, Stefan Klumpp, Eduard M Mateescu, and Terence Hwa. Emergence of robust growth laws from optimal regulation of ribosome synthesis. *Molecular Systems Biology*, 10(8):747, August 2014.

[22] M. Kaczanowska and M. Ryden-Aulin. Ribosome Biogenesis and the Translation Process in Escherichia coli. *Microbiology and Molecular Biology Reviews*, 71(3):477–494, September 2007.

[23] S. Klumpp, M. Scott, S. Pedersen, and T. Hwa. Molecular crowding limits translation and cell growth. *Proceedings of the National Academy of Sciences*, 110(42):16754–16759, October 2013.

[24] O. Maaløe. Regulation of the Protein-Synthesizing Machinery—Ribosomes, tRNA, Factors, and So On. In Robert F. Goldberger, editor, *Biological Regulation and Development: Gene Expression*, pages 487–542. Springer US, Boston, MA, 1979.

[25] John Yin. Genome Function—A Virus-World View. In Lee K. Opresko, Julie M. Gephart, and Michaela B. Mann, editors, *Advances in Systems Biology*, pages 31–46, Boston, MA, 2004. Springer US.

[26] R. E. Ecker and M. Schaechter. BACTERIAL GROWTH UNDER CONDITIONS OF LIMITED NUTRITION*. *Annals of the New York Academy of Sciences*, 102(3):549–563, December 2006.

[27] Alon Zaslaver, Shai Kaplan, Anat Bren, Adrian Jinich, Avi Mayo, Erez Dekel, Uri Alon, and Shalev Itzkovitz. Invariant Distribution of Promoter Activities in Escherichia coli. *PLoS Computational Biology*, 5(10):e1000545, October 2009.

[28] R J Harvey. Fraction of Ribosomes Synthesizing Protein as a Function of Specific Growth Rate. 114:7, 1973.

[29] N. O. Kjeldgaard, O. MaalOe, and M. Schaechter. The Transition Between Different Physiological States During Balanced Growth of Salmonella typhimurium. *Journal of General Microbiology*, 19(3):607–616, December 1958.

[30] Moselio Schaechter. From growth physiology to systems biology. *International Microbiology*, 9(3):157–161, 2006.

[31] M. Scott, C. W. Gunderson, E. M. Mateescu, Z. Zhang, and T. Hwa. Interdependence of Cell Growth and Gene Expression: Origins and Consequences. *Science*, 330(6007):1099–1102, November 2010.

[32] Hans Bremer and Patrick P Dennis. Modulation of Chemical Composition and Other Parameters of the Cell by Growth Rate. page 27.

[33] A H Stouthamer and Corry Bettenhaussen. CONTINUOUS AND BATCH CULTURES OF MICROORGANISMS. page 18.

[34] Christine Miller, Line Elnif Thomsen, Carina Gaggero, Ronen Mosseri, Hanne Ingmer, and Stanley N Cohen. SOS response induction by \textbackslashs s-lactams and bacterial defense against antibiotic lethality. *Science*, 305(5690):1629–1631, 2004.

[35] T Ruusala, D Andersson, M Ehrenberg, and C G Kurland. Hyper-accurate ribososomes inhibit growth. page 6.

[36] David W. Adams and Jeff Errington. Bacterial cell division: assembly, maintenance and disassembly of the Z ring. *Nature Reviews Microbiology*, 7(9):642–653, September 2009.

[37] Lydia Robert. Size sensors in bacteria, cell cycle control, and size control. *Frontiers in Microbiology*, 6, May 2015.

[38] Ingvild Flåtten, Solveig Fossum-Raunehaug, Riikka Taipale, Silje Martinsen, and Kirsten Skarstad. The DnaA Protein Is Not the Limiting Factor for Initiation of Replication in Escherichia coli. *PLOS Genetics*, 11(6):e1005276, June 2015.

[39] Erfei Bi and Joe Lutkenhaus. FtsZ ring structure associated with division in Escherichia coli. *Nature*, 354(6349):161–164, November 1991.

[40] Bill Söderström, Alexander Badrutdinov, Helena Chan, and Ulf Skoglund. Cell shape-independent FtsZ dynamics in synthetically remodeled bacterial cells. *Nature Communications*, 9(1):4323, 2018.

[41] Parth Pratim Pandey and Sanjay Jain. Analytic derivation of bacterial growth laws from a simple model of intracellular chemical dynamics. *Theory in Biosciences*, 135(3):121–130, September 2016.

[42] Jacques Monod. THE GROWTH OF BACTERIAL CULTURES. page 24.

[43] Johan Elf, Karin Nilsson, Tanel Tenson, and M\textbackslasha ans Ehrenberg. Bistable bacterial growth rate in response to antibiotics with low membrane permeability. *Physical Review Letters*, 97(25):258104, 2006.

[44] P. Greulich, M. Scott, M. R. Evans, and R. J. Allen. Growth-dependent bacterial susceptibility to ribosome-targeting antibiotics. *Molecular Systems Biology*, 11(3):796–796, March 2015.

[45] Leigh K. Harris and Julie A. Theriot. Surface Area to Volume Ratio: A Natural Variable for Bacterial Morphogenesis. *Trends in Microbiology*, 26(10):815–832, October 2018.

[46] Daan H. de Groot, Julia Lischke, Riccardo Muolo, Robert Planqué, Frank J. Bruggeman, and Bas Teusink. The common message of constraint-based optimization approaches: overflow metabolism is caused by two growth-limiting constraints. *Cellular and Molecular Life Sciences*, November 2019.

[47] Matteo Mori, Terence Hwa, Olivier C. Martin, Andrea De Martino, and Enzo Marinari. Constrained Allocation Flux Balance Analysis. *PLOS Computational Biology*, 12(6):e1004913, June 2016.

[48] Markus Basan, Sheng Hui, Hiroyuki Okano, Zhongge Zhang, Yang Shen, James R. Williamson, and Terence Hwa. Overflow metabolism in Escherichia coli results from efficient proteome allocation. *Nature*, 528(7580):99–104, December 2015.

[49] Bastian Niebel, Simeon Leupold, and Matthias Heinemann. An upper limit on Gibbs energy dissipation governs cellular metabolism. *Nature Metabolism*, 1(1):125–132, January 2019.

[50] Tobias Bollenbach, Selwyn Quan, Remy Chait, and Roy Kishony. Nonoptimal Microbial Response to Antibiotics Underlies Suppressive Drug Interactions. *Cell*, 139(4):707–718, November 2009.

[51] Ana Rita Brochado, Anja Telzerow, Jacob Bobonis, Manuel Banzhaf, André Mateus, Joel Selkrig, Emily Huth, Stefan Bassler, Jordi Zamarreño Beas, Matylda Zietek, and others. Species-specific activity of antibacterial drug combinations. *Nature*, 559(7713):259, 2018.

[52] Guillaume Chevereau, Marta Dravecká, Tugce Batur, Aysegul Guvenek, Dilay Hazal Ayhan, Erdal Toprak, and Tobias Bollenbach. Quantifying the Determinants of Evolutionary Dynamics Leading to Drug Resistance. *PLOS Biology*, 13(11):e1002299, November 2015.

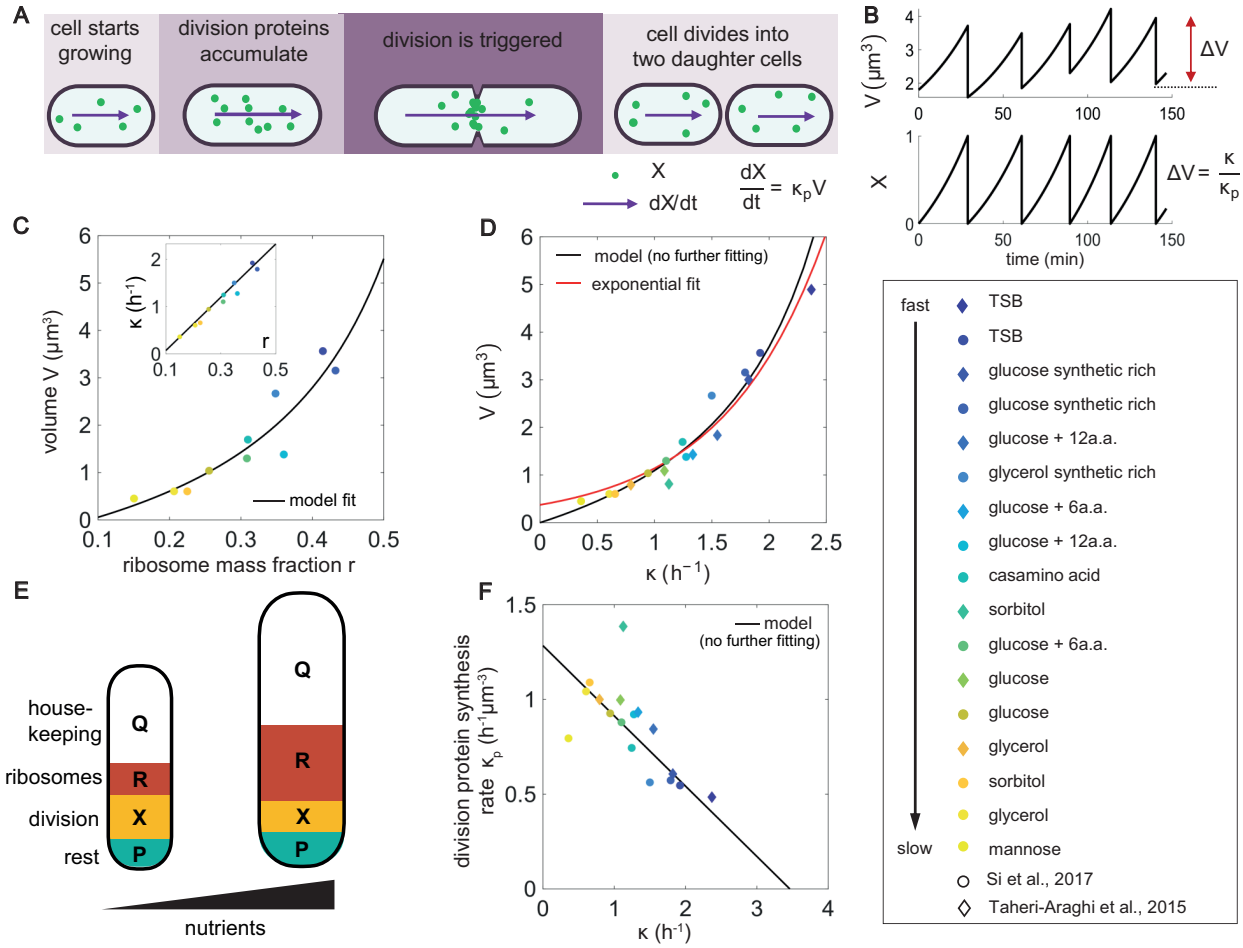

Figure 1. **Cell size control under nutrient perturbations. A.** Schematic of the threshold initiation model. Once a threshold amount of division proteins, X, is accumulated, cell division is triggered. Division proteins are synthesized at a rate κ_p per unit volume. **B.** Dynamics of cell volume and fraction of division proteins show that the average added volume between consecutive division events is constant, consistent with the phenomenological adder model [4]. **C.** Fitted model for average cell volume as a function of ribosome mass fraction. Inset: fitted linear relationship $\kappa = \kappa_t(r - r_{\min})$ [31]. **D.** Model prediction for the relationship between the average volume and growth rate compared against an exponential fit as predicted by the nutrient growth law [2]. **E.** Schematic representation of the proteome allocation model, showing ribsomal tradeoff between cell growth and division protein synthesis for cells growing in poor and rich nutrient media. **F.** Negative correlation between the rate of division protein synthesis and growth rate, as predicted by the model. Experimental data are obtained from Si *et al.* [4] and Taheri-Araghi *et al.* [5]. In the experimental data κ_p is estimated from the ratio $\kappa/\langle V \rangle$. See Table 1 for a complete list of parameter values.

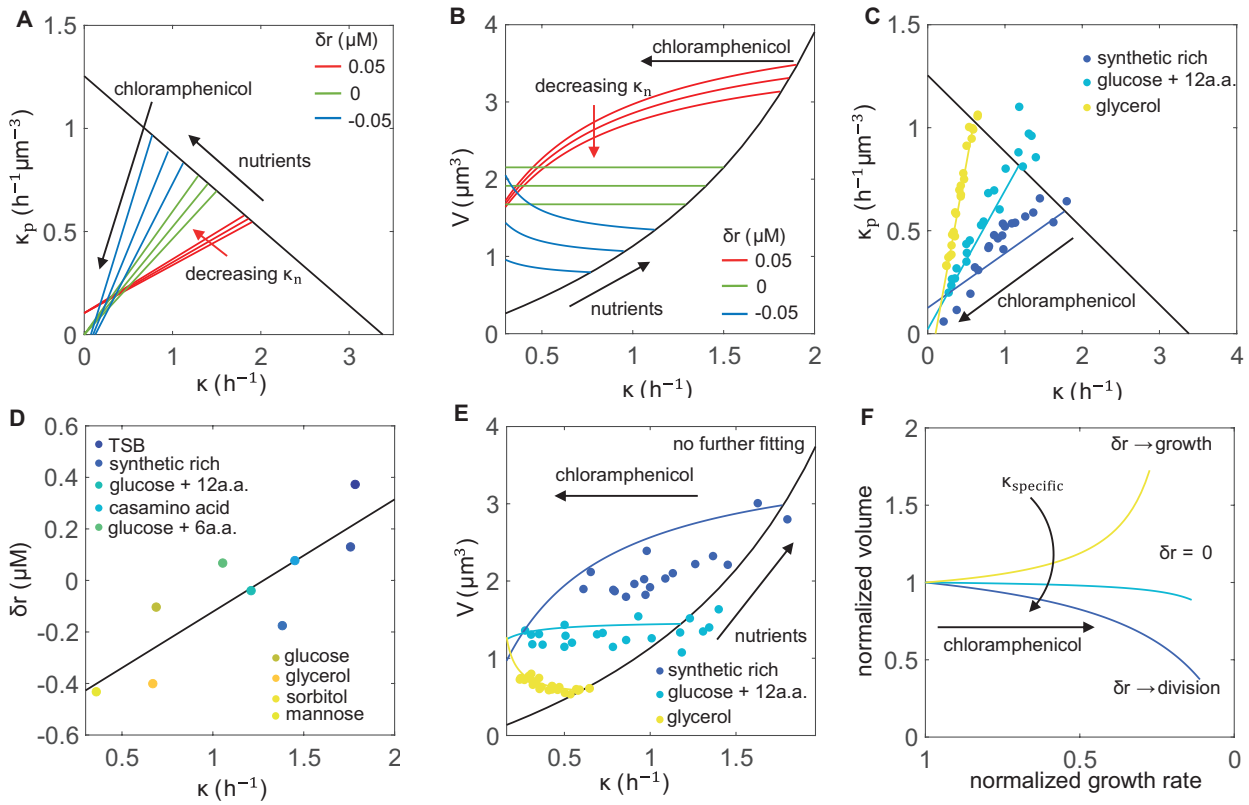

Figure 2. **Cell size control under translation inhibition. A.** Model prediction for the dependence of division protein synthesis rate, κ_p, on growth rate, κ, under translation inhibition for three different values of δr. Decreasing κ_n corresponds to increasing the nutrient quality of the growth medium. **B.** Model predictions for cell volume vs growth rate under translation inhibition, capturing three distinct trends in cell size changes depending on the value of δr. **C.** Model fit to experimental data for κ_p as a function of κ in three different nutrient conditions under translation inhibition. **D.** Dependence of δr on nutrient specific growth rate. **E.** Cell volume changes with growth rate under translation inhibition. **F.** Schematic illustrating three distinct morphological response to Chloramphenicol, depending on the quality of nutrients. In nutrient-rich media, cells allocate more ribosomes to division (dark blue line) thus increasing the surface-to-volume ratio to promote nutrient influx, while in nutrient-poor media they allocate the more ribosomes towards growth, inflating the cell size (yellow line) and in turn decreasing the surface-to volume ratio to reduce the antibiotic influx. See Table 1 for a complete list of parameter values.

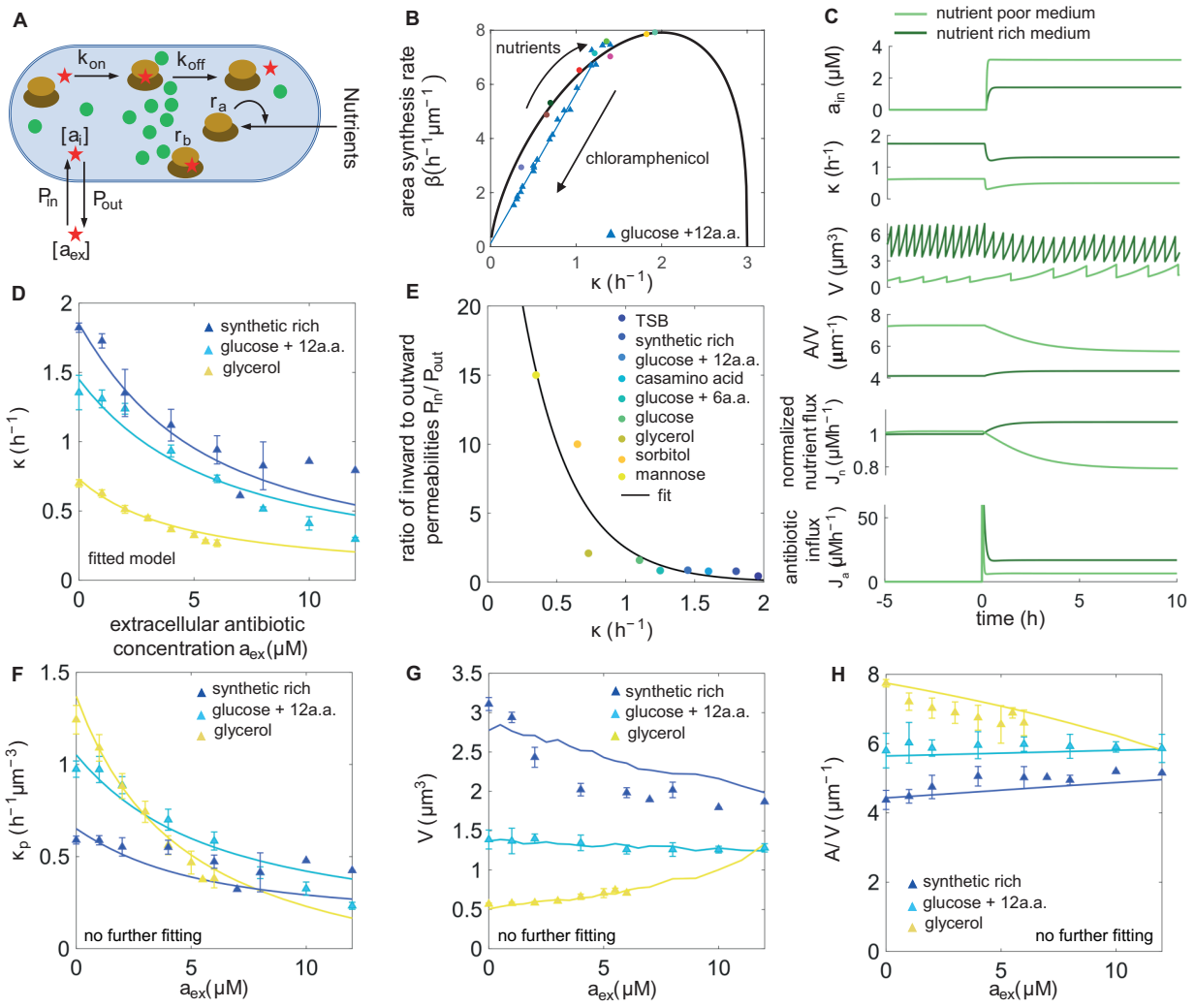

Figure 3. **Cell shape control under translational inhibition. A.** Schematic illustrating nutrient and antibiotic transport across cell surface and antibiotic interactions inside the cell. **B.** Model predictions for the surface area synthesis rate (β) as a function of the growth rate (κ) for varying nutrient conditions, and its inhibition under Chloramphenicol perturbations. β is calculated using $\beta = \kappa A/V$. **C.** Single-cell simulations of growth in response to a step pulse of Chloramphenicol applied at $t = 0$ h in the extracellular medium. Top to bottom: Dynamics of intracellular antibiotic concentration, growth rate, cell volume, surface-to-volume ratio, normalized nutrient and antibiotic flux. Both nutrient and antibiotic fluxes are higher in rich media due to the increase in surface-to-volume ratio. **D.** Model growth inhibition curves fitted to experimental data [4], in order to deduce the ratio of inward to outward cell-surface permeability. **E.** $P_{\text{in}}/P_{\text{out}}$ increases with decreasing growth rate (quality of nutrients). We used an exponential fit to calibrate $P_{\text{in}}/P_{\text{out}}$ for different nutrient conditions. **F-H.** Simulation results for the dependence of κ_p (F), average cell volume V (G), and average cell surface-to-volume ratio A/V (H) on Chloramphenicol concentration, plotted against experimental data [4] at three different nutrient conditions. Error bars represent standard error of the mean. See Tables 1 and 2 for a complete list of parameter values.

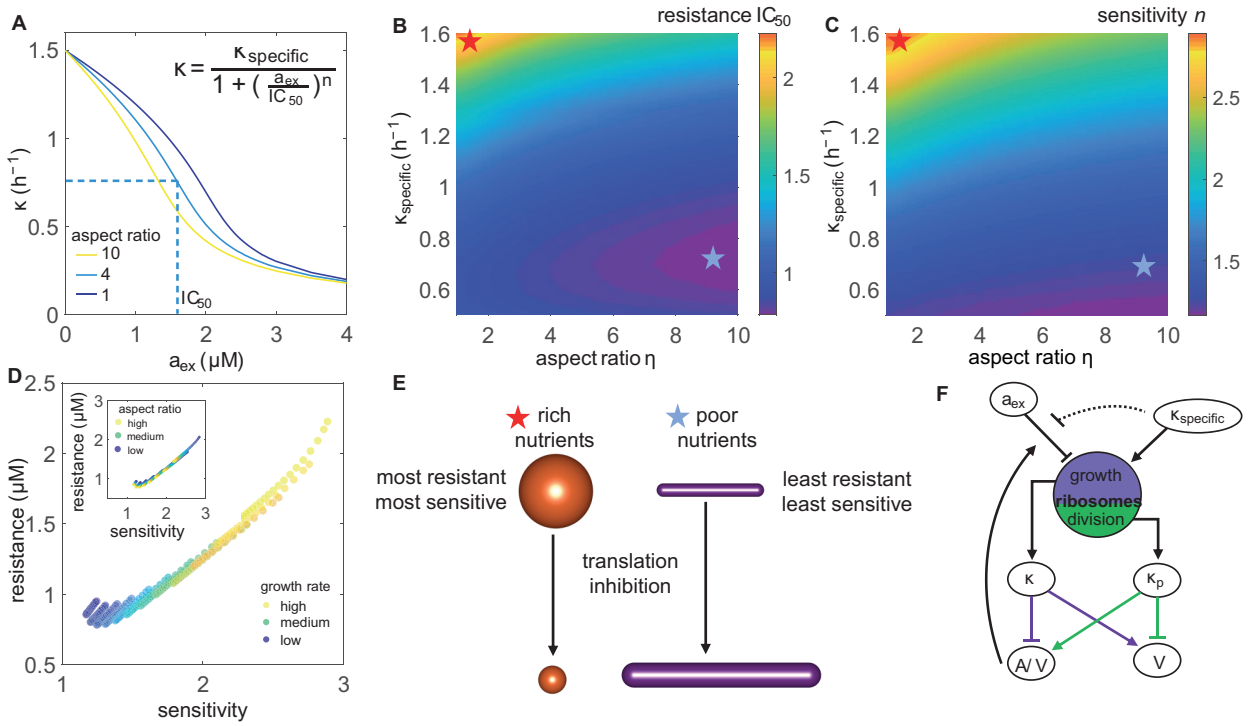

Figure 4. **Cell shape and nutrient quality control bacterial resistance to ribosome-targeting antibiotics**. **A.** Growth inhibition curves for three different values of cell aspect ratio in a nutrient-rich medium. Dashed line corresponds to IC_{50} on the x-axis, the concentration of antibiotic when the growth rate reduces by half. **B.** Heatmap of IC_{50}, a metric for drug resistance, showing the effects of changing aspect ratio and nutrient quality. Red asterix: Maximally resistant, blue asterix: least resistant. **C.** Heatmap of drug dose-sensitivity (n), showing the effects of changing cellular aspect ratio and nutrient quality of the growth medium. **D.** Correlation between drug resistance and dose-sensitivity under changes in nutrient quality (κ_{specific}). Inset: Correlation between drug resistance and dose-sensitivity under changes in aspect-ratio. **E.** Schematic illustrating fitness value for cell shapes and morphological changes that accompany bacterial response to translation inhibition in nutrient-rich and nutrient-poor growth media. **F.** Schematic representation of the feedback pathways that connect ribosomal translation to bacterial cell shape, growth, nutrient and antibiotic transport. See Tables 1 and 2 for a complete list of parameter values.